

Patrick Crotty

Department of Physics, University of Chicago, Chicago, Illinois 60637

prcrotty@oddjob.uchicago.edu

(Dated: May 13, 2002)

We calculate the fluxes and energy spectra of high-energy ( $E > 50$  GeV) neutrinos from the annihilations of supermassive ( $10^8$  GeV  $< M < 10^{16}$  GeV), strongly interacting dark matter particles in the core of the Sun. We take all significant aspects of neutrino propagation through matter into account, as well as oscillations in matter and vacuum. We also calculate the resulting event rates in an idealized 1 km<sup>3</sup> ice detector. We find that the signal should be well above background and easily observed by next-generation neutrino detectors such as IceCube.

PACS numbers: 13.15.+g, 14.60.Pq, 95.35.+d

## I. INTRODUCTION

The identity of the non-baryonic dark matter, believed to account for about 30% of the total density of the Universe [1], is one of the major unanswered questions in cosmology today. There is much speculation that the dark matter consists of massive non-Standard Model elementary particles. The so-called "wimp," or weakly interacting massive particles, are the best known such candidate. These are often taken as the lightest supersymmetric particle, with a mass of no more than about 7 TeV [2]. Any dark matter particle which is a thermal relic cannot have a mass of more than about 340 TeV [3]. It has been shown that wimps could be captured by the Sun [4, 5], and that their subsequent annihilations could produce an observable flux of high-energy neutrinos [6].

Recently, another candidate for particle dark matter has been proposed, the "simps" [7, 8, 9, 10, 11]. These are gravitationally produced towards the end of inflation by the interaction of the wimp field with the inflating space-time, and in sufficient abundance to be the dark matter. The wimp is usually not assumed to be coupled to any other fields, although the case of coupling between the wimp and the inflaton has been studied and wimp production still found to be robust [12]. The original calculations were done in the context of chaotic inflation ( $V(\phi) = \frac{1}{2}m^2\phi^2$ ), but wimp-simps have been shown to be abundantly produced for other inflaton potentials too [13]. Wimp-simps are most efficiently produced at extremely high masses, on the order of  $10^{12}$  GeV.

A crucial difference between wimps and wimp-simps is that the latter are never in thermal equilibrium, and as such, their masses are not thermodynamically constrained. It also follows from this that their present-day abundance does not depend on whether they have strong, weak, electromagnetic, or only gravitational interactions (although there are other considerations which generally rule out charged dark matter [14, 15]).

We assume in this paper that the non-baryonic dark matter consists of wimp-simps with strong interactions, referred to from now on as "simps." Simps, like thermal wimps, can be captured by the Sun, and their

annihilations in the solar core can produce high-energy neutrinos. We present the results of a detailed Monte Carlo calculation simulating the propagation of high-energy neutrinos from simps annihilations through the Sun, and also taking oscillations in matter and vacuum into account.

Our general conclusion is that the flux of high-energy neutrinos from simps annihilations should be well above background for a broad range of parameter space, and observable by next-generation neutrino detectors such as IceCube.

## II. INITIAL NEUTRINO FLUX

Abuquerque, Hui and Kolb [16], henceforth AHK, derived the capture rate of simps by the Sun. The capture of thermal wimps by the Sun had previously been studied in [4, 5]. AHK assumed that the dark matter consists entirely of simps in a Maxwell-Boltzmann velocity distribution, and that the interaction cross section is of the order of the strong force, implying that the Sun is many interaction lengths thick. AHK's formulas for the capture rate are given in equations (2.5) and (2.7) of their paper. We plot the capture rate  $c$  in Figure 1. The capture rate has two different forms, determined by the efficiency of the simps energy loss in the Sun.

Once captured by the Sun, the simps rapidly fall to the core and annihilate with each other. AHK showed that equilibrium between annihilation and capture is reached very early in the lifetime of the Sun, and would obtain today. In equilibrium, by definition,  $A = c = 2$  (each annihilation destroys two simps). Note that this has the effect of making the equilibrium value of  $A$  dependent only on the interaction cross section and not the annihilation cross section  $A$ .

High-energy neutrinos are produced by the simps annihilations, which produce a quark or gluon pair that then fragment into hadronic jets containing a large number of particles. AHK used the fragmentation function formalism of [17] to calculate the numbers of hadrons produced per annihilation. In the dense solar core, hadrons

composed of light and charm quarks lose most of their energy before decaying. Hadrons with bottom and top quarks, however, have much shorter lifetimes and decay before substantial energy losses. The neutrinos from these decays are at high energies.

In this paper, as AHK did, we consider the high-energy neutrinos from top hadrons produced in simpzilla annihilations. Although high-energy neutrinos can also come from bottom hadrons, it is generally quite difficult to calculate their flux due to the large number of B meson decay modes, the products of which may interact in the Sun before themselves decaying. Since we find that the neutrino flux from top hadron decays alone is well above background, including the neutrinos from B decays will only add to an already detectable signal, although most of these will be below the 50 GeV cut-off energy we choose.

Approximately  $2.8 \cdot 10^5 M_{12}^p$  top hadrons are produced per simpzilla annihilation, where  $M_{12} = 10^{12}$  GeV. Top quarks almost always decay in the channel  $t \bar{t}$ . The  $W$ , in turn, decays with equal branching ratios (each about 10.5%) into  $e^+$ ,  $e^-$ , and

$\nu_e$ . The  $W$ , like the  $t$ , decays before virtually any energy loss. When the  $t\bar{t}$  pair is produced by the  $W$  decay, the  $t$  also decays before losing much energy, producing a second  $W$ . About 18% of the time, it also produces a second  $e^+$  and another 18% of the time a second  $e^-$ .

AHK showed that the top hadrons have an energy distribution proportional to  $E^{-3/2}$ . They also calculated the distribution of the subsequent neutrinos. The total number of neutrinos produced above 50 GeV from this  $t\bar{t} \rightarrow W \rightarrow t\bar{t}$  decay chain is

$$\frac{d\Gamma}{dt} = 1.10^4 M_{12}^p \frac{1}{A}; \quad (2.1)$$

where  $\Gamma$  denotes the neutrino flavor ( $e^+$ ,  $e^-$ , or  $\nu_e$ ).  $\Gamma = 1$  for  $\nu_e$  and  $\Gamma = 2$  for the other two flavors, representing the fact that roughly twice as many  $\nu_e$  are produced per annihilation.

The initial neutrino energy distribution calculated by AHK is

$$\frac{d\Gamma}{dE dt} = 1.10^4 M_{12}^p \frac{1}{A} \frac{E_{\text{min}}}{E + m_W} \frac{0.939}{\frac{E + m_t}{m_t^2} \frac{1}{(E + m_t)^2} + \frac{E + m_W}{m_W^2} \frac{1}{(E + m_W)^2}} \quad (2.2)$$

Here,  $E_{\text{min}} = 50$  GeV. This is near the lower limit of energies detectable by IceCube [18], and also roughly the lowest neutrino energy possible in the two-body  $W$  decay.

In Figure 2, we show the initial simpzilla neutrino flux at the core of the Sun.

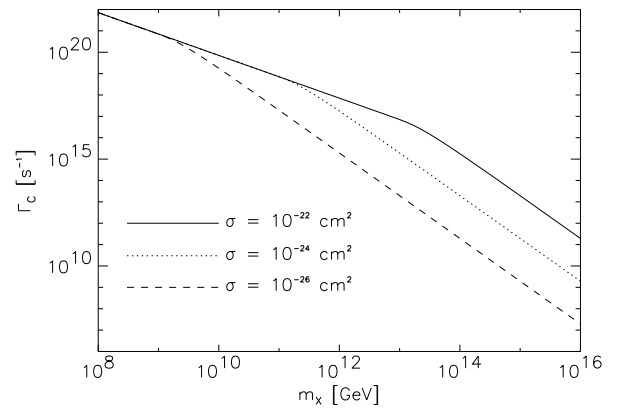


FIG. 1: The capture rate of simpzillas by the Sun as a function of simpzilla mass  $m_x$ , for three different choices of the interaction cross section  $\sigma$ . In the shallower parts of the curves, most of the simpzillas are captured. In the steeper parts, the simpzilla energy loss in the Sun is efficient and only those with lower velocities are captured.

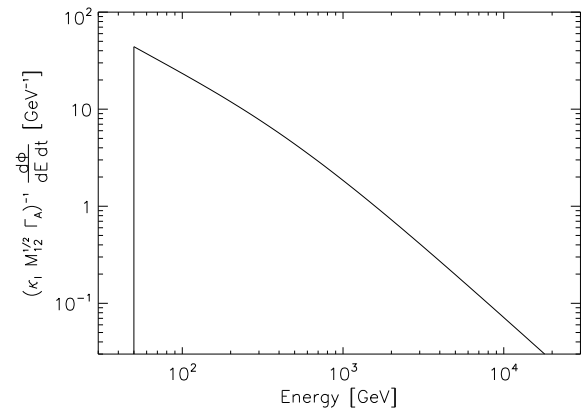


FIG. 2: The initial energy distribution of neutrinos from top hadrons produced in simpzilla annihilations.  $\Gamma = 1$  for  $\nu_e$  and  $\Gamma = 2$  for  $e^+$  and  $e^-$ . Note that the typical neutrino energy is much lower than the simpzilla mass, due to the large numbers of neutrinos produced per annihilation.

### III. NEUTRINO INTERACTIONS

Neutrinos with energies above about 100 GeV have significant interactions with matter as they propagate through the Sun. The majority are charged-current (CC) interactions with nucleons. The rest are neutral-current (NC) scatterings; the cross sections for the latter are about one-third of the charged-current scattering cross sections at the same energy. Neutrino-electron scatterings in this energy range are negligible compared to

neutrino-nucleon scatterings<sup>1</sup> [19], and accordingly we do not consider them in our code.

We have calculated the charged and neutral-current neutrino-nucleon cross sections between 1 GeV and  $10^9$  GeV. The most recent previous calculations in this energy range [19, 20] have assumed an isoscalar nucleon; that is, one in which the quark distribution functions are the average of those for the proton and neutron. This is a good approximation for a medium such as rock (the calculations were in the context of high-energy neutrino beams propagating through the Earth). However, the proton number density in the Sun is between two and six times the neutron number density, and the isoscalar approximation does not hold. We show the ratio of proton and neutron number densities in Figure 3, calculated using the Standard Solar Model of [21].

We have used the recently published CTEQ 6-L (leading order) parton distribution functions [22], together with the deep inelastic scattering formalism of [23], to calculate the cross sections. Given the energies involved, we may neglect the electron and muon masses, and so the  $e^-$  and CC cross sections are identical. The  $e^-$  mass, however, significantly suppresses the CC cross sections up to about 50 GeV. Although the effect of this on our calculation of the emergent supernova neutrino fluxes is minor (we only consider energies above 50 GeV, and neutrino interactions in the Sun are significant only above about 100 GeV), we have taken it into account. The NC cross sections are identical for all three flavors. We show our results in Figures 4-6.

Note that for  $E < 10^4$  GeV (and in the case of  $e^-$ , above energies where the mass suppression is significant), the cross sections are approximately proportional to energy. At higher energies, the rate at which the cross section increases is suppressed by the gauge boson propagator [19]. However, almost all of the supernova neutrino flux is below  $10^4$  GeV.

We have also calculated the differential cross sections  $d\sigma/dy$ , where the inelasticity parameter is

$$y = 1 - \frac{E^0}{E} \quad (3.1)$$

and  $E^0$  is the final charged lepton (neutrino) energy in a CC (NC) scattering. We show these for  $e^-$  and CC scattering in Figures 7 and 8; the others are similar. Our code uses these differential cross sections to obtain probability distributions for  $E^0$ .

We find numerically that almost all neutrino interactions take place in the deepest part of the Sun, where the density is greatest, out to about  $0.1R_\odot$ . This is significant when oscillations are taken into account, because at high energies the oscillations and interactions effectively decouple in radius (see section V).

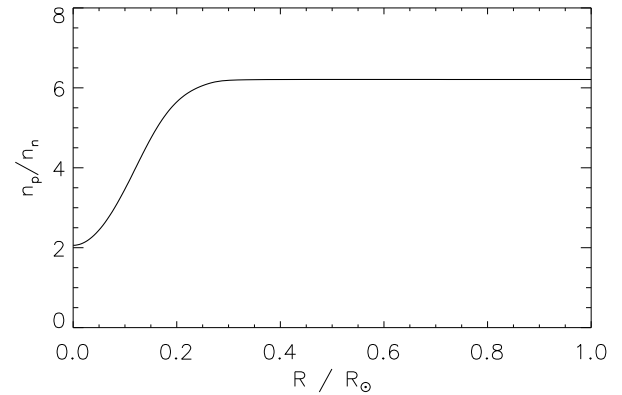


FIG. 3: The ratio of the proton and neutron number densities in the Sun as a function of radius. The number of neutrons is greatest in the core where more hydrogen has been processed into helium. Isotopes other than  $^1H$  and  $^4He$  are neglected.

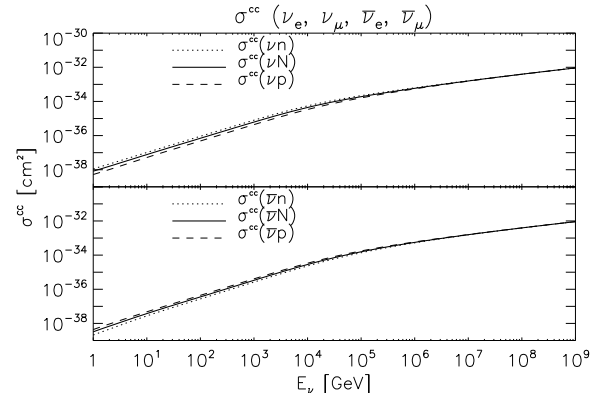


FIG. 4: The charged-current interaction cross section between an electron or muon neutrino and a neutron (n), proton (p), and isoscalar nucleon (N).

#### IV. CHARGED LEPTON INTERACTIONS

The charged leptons produced in charged-current interactions are very important in determining the emergent neutrino flux. Electrons and muons tend to be stopped by their electromagnetic energy losses. However, taus have very short lifetimes. They tend to decay before losing any significant fraction of their energy, and so the resulting taus are also high-energy. CC interactions, in effect, absorb the  $e^-$  and  $\tau^-$  but regenerate the  $\tau^+$ . This phenomenon was first remarked upon by Ritz and Seckel [6] in the context of a calculation of neutrino spectra from thermal leptopannihilation in the Sun (see also [24]); Halzen and Saltzberg [25] have shown it to obtain for high-energy neutrino beams propagating through the Earth (see also [26, 27, 28]).

In the absence of oscillations, this means that high-

<sup>1</sup> Except for  $e^-$  in the vicinity of the Glashow resonance at 6.3 PeV. However, the fluxes we consider are far below this.

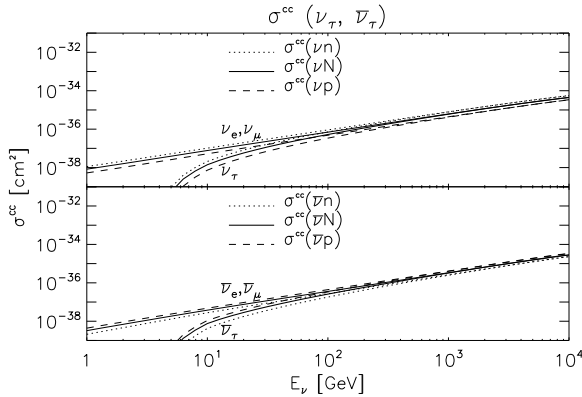


FIG. 5: The charged-current cross sections for a tau neutrino. The electron/μon neutrino cross sections are also shown to illustrate the kinematic suppression due to the mass.

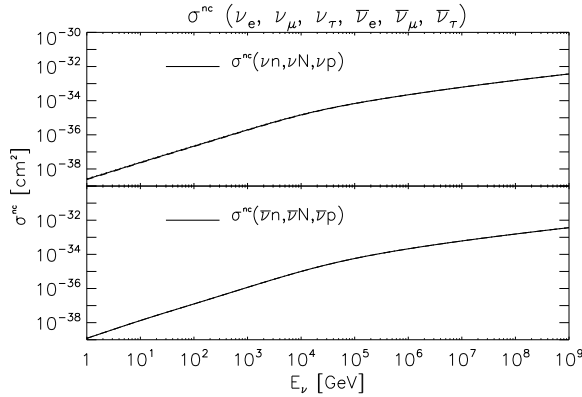


FIG. 6: The neutral-current cross sections for all three flavors.

energy are much more likely than high-energy  $e^-$  and to survive. The are moderated down to lower energies, to the point where the probability of further interactions is small. However, the total number of emerging is essentially equal to the initial number, whereas the  $e^-$  and  $e^+$  are attenuated. We will discuss the properties of the versus  $e^-$  emergent fluxes in greater detail in the penultimate section, including the effects of oscillations.

In this section, we consider the energy losses and decays of the charged leptons in the solar medium.

#### A. Energy losses

As the charged leptons move through the Sun, they have electromagnetic interactions with the medium and lose energy. Weak interactions, apart from decays, are insignificant for charged leptons at energies below

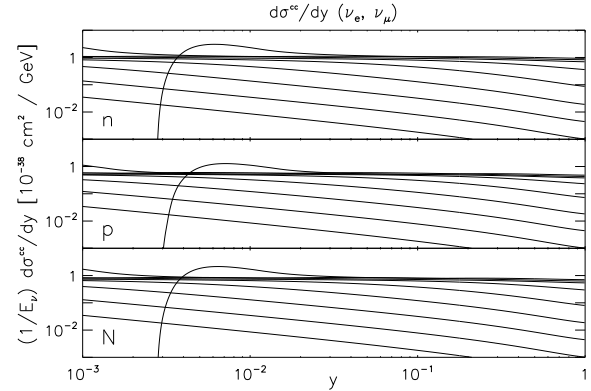


FIG. 7: CC differential cross sections for a  $e^-$  or  $\mu^-$ . From top to bottom at  $y = 5 \cdot 10^{-3}$ , the curves correspond to  $10 \text{ GeV}, 10^2 \text{ GeV}, \dots, 10^9 \text{ GeV}$ . The cuts in the  $10 \text{ GeV}$  curves at  $y \gtrsim 10^{-3}$  are where the  $Q^2$  of the gauge boson decreases below  $Q_{\text{CD}}^2$ , and hence the parton formalism used to calculate deep inelastic scattering becomes invalid.

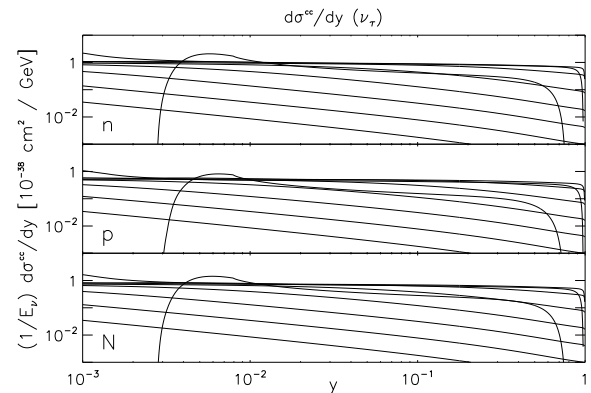


FIG. 8: CC differential cross sections for a  $\tau^-$ . The energies are the same as in Figure 7. The cuts at large  $y$  in the  $10 \text{ GeV}$  and  $100 \text{ GeV}$  curves are due to the mass.

$10^{16} \text{ GeV}$  [29]). The general equation for energy loss as a function of column depth  $x$  is

$$\frac{dE}{dx} = - \frac{X}{\sum_j j E_j}; \quad (4.1)$$

where  $E$  represents interactions with electrons and  $E_j$  represent interactions with nuclei, with the summation being over the different processes: bremsstrahlung, pair production, and photonuclear scattering. Below  $10^4 \text{ GeV}$ , where most of the sun's neutrinos (and charged leptons from their CC scatterings) are produced, electronic losses dominate. In most terrestrial situations, these are ionization losses which can be calculated with the Bethe-Bloch formula [30, 31], but inside the Sun the electrons are unbound. Therefore,  $E$  is the energy loss

rate of a charged particle in a plasma [6],

$$= 9.2 \cdot 10^6 \frac{Z}{A^2 c} \ln(2m_e^2) \ln \frac{r}{m_e} \quad : \quad (4.2)$$

The units of  $\ln$  in Eq. (4.2) are  $\text{GeV} = (\text{g} \cdot \text{cm}^2)$ . The quantities  $Z$  and  $A$  are the atomic number and weight of the nuclei in the medium (for the Sun, which is approximately a mixture of  $^1\text{H}$  and  $^4\text{He}$ , we calculate the energy losses separately for the two isotopes and then weight them by their mass fractions. The  $\gamma$  and  $\mu$  are the Lorentz parameters of the charged lepton and  $n_e$  is the electron number density.

The nuclear energy losses become dominant at energies above about  $10^4 \text{ GeV}$ , although as mentioned they are not very important for the simple neutrino flux which tends to be at energies below this. The formulas for  $\gamma$  and  $\mu$  are given, for example, in [29].

Our code simulates both electronic and nuclear energy losses for  $\mu$  and  $\tau$ . We do not follow  $e$  since they never decay. In Figure 9, we show the muon and tau ranges and decay lengths in the core of the Sun, which is where the majority of neutrino interactions take place. The range is defined as the distance, in the absence of decays, over which the lepton would lose all its energy; and similarly the decay length is the (mean) distance, in the absence of energy losses, the lepton would travel before decaying.

## B. Decays

Both muons and taus decay back into neutrinos, but the muons have lost almost all their energy by this point and essentially decay at rest. The resulting  $\nu$  are below  $50 \text{ MeV}$  and do not concern us. The taus, on the other hand, have negligible energy losses except at very high energies ( $E > 10^7 \text{ GeV}$ ), which again does not concern us since very little of the initial simple neutrino flux is in this range. The  $\nu$  from the decay carries on average about  $2/5$  the energy of the  $\tau$ , or about  $1/4$  the energy of the incident  $\tau$  (the mean energy of the  $\tau$  relative to the incident  $\tau$  can be obtained from the inelasticity parameter distributions; in the energy range we consider, the mean value of  $y$  is about 0.4, higher than for the energies at which neutrinos interact significantly in the Earth).

One phenomenon our code takes into account is the production of secondary  $e$  and  $\nu$  in decays, as discussed by [28]. Approximately 18% of decays produce a  $\nu_e$  (for  $\tau \rightarrow \nu_e$ , a  $\nu_e$ ), and another 18% produce a  $\bar{\nu}_e$ . These secondary neutrinos are created with about half the energy of the accompanying  $\nu$ , or about  $1/8$  the energy of the incident  $\tau$ . When the  $\tau$  experiences its last few charged-current scatterings and is downscattered to energies at which it escapes the Sun, these secondary neutrinos emerge too. Ref. [28] considered high-energy

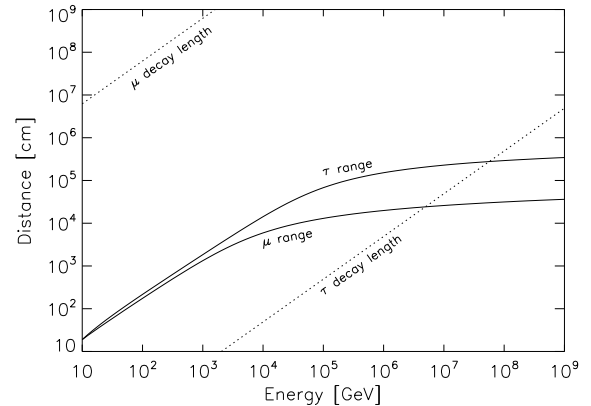


FIG. 9: Decay lengths and ranges of  $\mu$  and  $\tau$  in the solar core (where most charged-current interactions take place). Note that except at the highest energies, the decay length is much shorter than its range; hence it decays before losing virtually any energy. The opposite is true for the  $\tau$ , which is essentially brought to rest before decaying.

neutrino beams from extragalactic point sources propagating through the Earth, and showed that the additional flux of secondaries could substantially modify the detected signal.

The major decay channels of  $\tau$  are  $\tau \rightarrow e \bar{\nu}_e$  (18%);  $\tau \rightarrow \mu \bar{\nu}_\mu$  (18%);  $\tau \rightarrow \nu_\tau \bar{\nu}_\tau$  (12%);  $\tau \rightarrow \bar{\nu}_\tau \nu_\tau$  (26%);  $\tau \rightarrow a_1$  (13%); and  $\tau \rightarrow X$  (13%), where  $X$  indicates other massive hadrons. The combined decay distribution is given in [29]. We show it in Figure 10, along with that of the secondary  $e$  and  $\nu$ , which is straightforward to obtain (see e.g. [32]). Our code randomly samples over the appropriate distributions to obtain the energies of the neutrinos from decays.

## V. NEUTRINO OSCILLATIONS

Both matter and vacuum oscillations are significant for simple neutrinos, and have a large effect on the emergent flux. Our code takes the oscillations of all three flavors into account. We use values for the mass-squared differences and mixing angles which are consistent with recent observations. From the SuperKamiokande results [33, 34], we choose  $m_{31}^2 = 3 \cdot 10^{-3} \text{ eV}^2$ ,  $\sin^2 \theta_{21} = 0.1$  (which is the upper limit on  $\theta_{21}$ ), and  $\sin^2 \theta_{13} = 0.5$ , where the angles in the three-flavor mixing matrix are as in Eq. (3.1) of [35]. The other parameters are constrained by solar neutrino observations, such as those recently recorded by the Sudbury Neutrino Observatory (SNO) [36, 37, 38]. Analysis of the SNO data favors the "large mixing angle" (LMA) solution [39], and so we choose values characteristic of this:  $m_{21}^2 = 2 \cdot 10^{-5} \text{ eV}^2$  and  $\sin^2 \theta_{12} = 0.2$ . We assume the normal mass hierarchy with  $m_1 < m_2 < m_3$ , and set the CP-violating phase in the mixing matrix to 0.

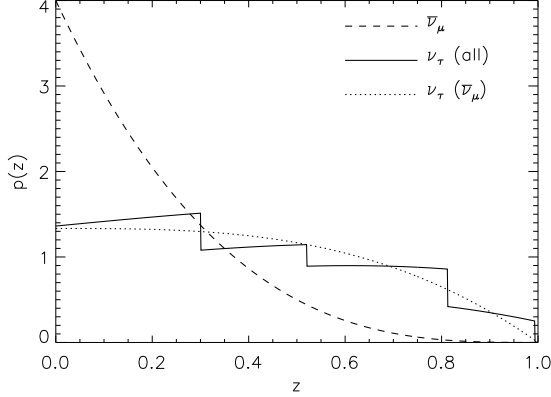


FIG. 10: Distributions of neutrino energies from decays, with  $z = E$  and the assumed to be ultrarelativistic. Solid curve: energy distribution, summing over all significant decay channels of the and weighting by the branching ratios. Some of the channels produce massive hadrons and become kinematically impossible above a certain  $z$ , the reason for the jagged appearance. Dashed curve: secondary and  $e^-$  decay distributions from the 18% of decays which produce them. Dotted curve: the energy distribution in the secondary-producing channels. We assume the to have the parity it would have if produced in a CC interaction (for  $e^-$ , negative; for  $e^+$ , positive).

To simulate the oscillations, we evolve the flavor amplitudes using the analytical solution for the time-evolution operator in [40, 41]. Our Monte Carlo step sizes are sufficiently small that the oscillation probabilities do not change significantly over the step, and the density at each step may be taken as constant. If the neutrino is determined to have had a charged-current interaction during the step, we sample over the current probabilities to find the flavor of the resulting charged lepton; if the lepton subsequently decays at high energy, the resulting neutrino begins purely in that flavor.

In Figures 11 and 12, we show the oscillation probabilities of 100 GeV neutrinos and antineutrinos traveling through the Sun without interacting (so their energies do not change). This is roughly the lower limit of where neutrino interactions in the Sun are significant.

We have noted above that most neutrino interactions take place between the center of the Sun and  $0.1R_\odot$ . At higher energies, the oscillation wavelengths increase, to the point where the oscillation probabilities do not vary substantially over this distance. Interactions at energies much greater than 100 GeV thus effectively "decouple" in radius from oscillations.

We also would not expect different reasonable choices of the oscillation parameters to make a difference of more than a factor of two or so in the detection rates. Real-world detectors most easily observe the muons created in and charged-current interactions (the  $e^-$  and signals are much less directional), so the relevant issue is how much different parameter choices would change the

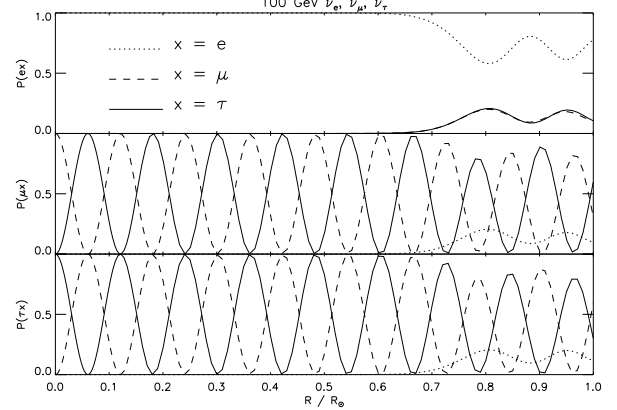


FIG. 11: Oscillation of 100 GeV neutrinos propagating (without interactions) from the center of the Sun to its surface. From top to bottom: oscillation probabilities of  $e^-$ ,  $\mu$ , and  $\tau$ . Note that the oscillations of  $e^-$  are almost completely suppressed until the resonance.

emergent  $e^- + \bar{\nu}_e$ . As can be seen from Figures 11 and 12, the worst-case scenario would completely deplete the flux by maximizing the  $e^-$  conversion probabilities; however, the flux would be unaffected since the  $e^-$  do not encounter a resonance and barely oscillate. (A difference in the sign of  $m_{31}^2$ , which is currently unknown and which we assume to be positive, would cause the  $e^-$  rather than the  $e^+$  to have a resonance, so the graphs would essentially be interchanged.)

The  $\delta$  oscillations in the Sun are vacuum oscillations with the atmospheric mixing parameters. The  $e^-$  resonance is governed by the mixing angle (corresponding to  $U_{e3}$ ) and  $m_{31}^2$ . This is in contrast to normal solar neutrinos, whose MSW resonance is governed by  $m_{21}^2$  and  $\delta$ . For the sunpzilla neutrinos, that resonance is in the outermost layers of the Sun at very low densities, and is not numerically significant compared to the other resonance. We note that vacuum oscillations outside the Sun are completely averaged out by the detector energy resolution (see section V I). We also note that although the detector is considered to be looking at upcoming sunpzilla neutrinos which have come through the Earth, the density of the Earth is too high for MSW oscillations inside it to be important.

## V I. NEUTRINO FLUX AT EARTH

Using the initial neutrino energy distribution given in (2.2) and taking all the physical effects discussed above into account, we have calculated the resulting neutrino flux at Earth. We have also, with IceCube in mind, calculated the event rates it would produce in an idealized  $1 \text{ km}^3$  ice detector.

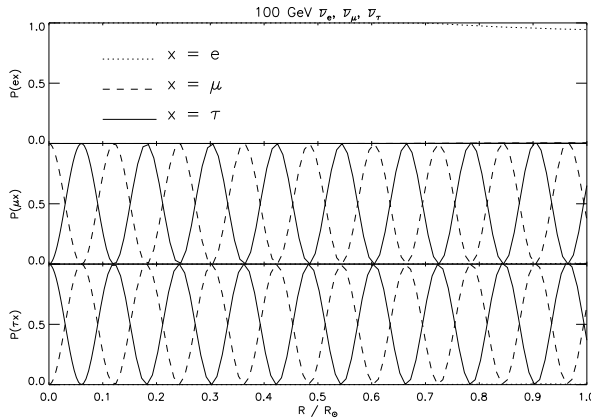


FIG. 12: Oscillations of 100 GeV antineutrinos propagating from the center of the Sun to its surface. The  $e$ , unlike the  $\mu$  and  $\tau$ , does not encounter a resonance, and its oscillations are minimal.

#### A. Monte Carlo code

We have written a Monte Carlo code to simulate the propagation of high energy neutrinos through matter. Each neutrino is followed as it passes through the Sun. The step sizes are chosen to be much smaller than both the interaction length and the neutrino oscillation length.

At each step, we use a pseudo-random number generator to determine whether an interaction occurred over that step, whether it was a charged- or neutral-current interaction, and whether it occurred on a proton or neutron. In the event of a neutral-current interaction, the final neutrino energy is determined by randomly sampling over the appropriate inelasticity parameter distribution (see section III).

Charged-current interactions are effectively measurements of the neutrino flavor. As such, when a charged-current interaction occurs, we randomly sample over the current oscillation probabilities to determine the flavor of the neutrino and outgoing lepton. When and if the lepton decays back into a neutrino, it starts in a pure flavor state. We calculate the initial energy of the lepton using the inelasticity parameter distribution.

The and produced in charged-current interactions are followed until they decay or their energies fall below 50 GeV. The  $e$  produced in  $e$  charged-current interactions are not followed since they never decay. (In practice, they almost never decay at high energies either, but we follow them for consistency.) We calculate their energy losses over each step according to (4.1). We also use their boosted decay lengths to randomly determine whether a decay occurs on each step. If so, we sample over the appropriate decay distribution to determine the energy of the outgoing neutrino. We also calculate the energies of the secondary  $e$  and  $\tau$  in decays using the energy distributions for those modes.

Neutrino oscillations are simulated both in the Sun

and in the vacuum between the Sun and the Earth. We average the oscillation probabilities over 10% of the Sun-Earth distance, which is mathematically equivalent to a 10% energy resolution in the detector (characteristic of real-world detectors).

The detector is considered to be able to detect every neutrino charged-current interaction above 50 GeV taking place in a cubic kilometer of ice. In practice, real detectors are considerably more complex than this and a sophisticated treatment would require a detector Monte Carlo, which is beyond the scope of this work. The detector is also assumed to have an angular resolution of 1°, which is approximately the size of the Sun on the sky.

Having calculated the neutrino flux at the Earth, we calculate the detection rate by integrating the product of the flux, the area of the detector ( $1 \text{ km}^2$ ), and the probability of the neutrino having a charged-current interaction, the integration being over the energy  $E$ . The probability of a charged-current interaction in the detector is

$$P_{\text{cc}}(E) = 1 - e^{-L_{\text{int}}(E)}; \quad (6.1)$$

with the interaction length

$$L_{\text{int}}(E) = \frac{1}{n_p \sigma_{\text{cc}}(E) + n_n \sigma_{\text{n}}(E)} \quad (6.2)$$

and  $= 1 \text{ km}$  is the size of the detector. The number densities  $n_n$  and  $n_p$  are for ice, and the charged-current cross sections  $\sigma_{\text{cc}}(E)$  were discussed in section III.

The background flux from atmospheric neutrinos above 50 GeV is approximately [42]

$$\frac{d\phi_{\text{atm}}}{dE dA dt d\Omega} = (1.1 \cdot 10^{12}) E^{-3.2} \text{ km}^{-2} \text{ yr}^{-1} \text{ deg}^{-2} \text{ GeV}^{-1}; \quad (6.3)$$

Integrating this over energy, the detection probability, the detector area, and the angular size of the Sun gives about 2 atmospheric neutrino events per year above 50 GeV which come from the direction of the Sun. These will be almost exclusively muon neutrinos, if we assume the detector is looking at incoming neutrinos. We take this as our background.

We also note that the Baksan neutrino telescope has placed a 90% confidence level limit of muon fluxes from nonatmospheric neutrinos coming from the direction of the Sun of about  $10^4 \text{ km}^{-2} \text{ yr}^{-1}$  [43]. We take this as a rough upper limit. The future analysis of the data from AMANDA [44] may lower this limit.

#### B. Results

In Figures 13 and 16, we show our numerical results for the simulation neutrino flux at the Earth. In Figures 17 and 18, we show the event rates as a function of simulation mass  $m_x$  for three different choices of the interaction cross section  $\sigma$ . We show two cases: when neither

oscillations nor secondaries are included, and when both are included. We have found that the secondaries alone do not make a dramatic difference to the flux, largely because it falls over several decades in energy, and much of it is in a region where neutrino interactions are not significant and thus secondaries are not produced. We accordingly do not show the other two permutations. Previously, only the case without oscillations or secondaries has been studied [16, 45].

We discuss this case briefly. As can be seen from Figure 13, the emergent fluxes exceed those of the other two flavors by more than the initial factor of 2 (see section II). This is due to the fact that the which experience charged-current interactions are not, as are the  $\nu_e$  and  $\nu_\mu$ , absorbed, but rather regenerated at lower energies, as remarked upon in section IV.

The unscattered components of the  $\nu_e$ ,  $\nu_\mu$ , and  $\nu_\tau$  beams relate to their initial fluxes as [16]

$$\frac{d\Phi_f}{dE dt} = \frac{d\Phi_0}{dE dt} e^{E=E_k}; \quad (6.4)$$

where  $E_k$  is the "transparency energy," defined as the energy such that the mean number of interactions experienced by the neutrino is 1. Equation (6.4) obtains because the cross sections are approximately linear functions of energy in the range we are considering. Numerically, we find that  $E_k = 130$  GeV for  $\nu_e$  and  $\nu_\mu$ ,  $160$  GeV for  $\nu_\tau$ ,  $200$  GeV for  $\nu_e$  and  $\nu_\mu$ , and  $230$  GeV for  $\nu_\tau$ . We use (6.4) as the emergent flux for the electron and muon neutrinos<sup>2</sup>.

To model the scattered component of the  $\nu_\tau$ , we use the observation of ourselves and several other groups that the scattered emerge in a roughly log-normal distribution. We find numerically that about 80% of the emergent and  $\nu_\tau$  are scattered. The log-normal distribution is defined as

$$\frac{dn}{dE} = \frac{1}{\sqrt{2 \ln 10} E} \exp \left( -\frac{1}{2} \log^2 \frac{E}{E_t} \right); \quad (6.5)$$

and when transformed to a distribution in  $\log E$ , is a Gaussian with mean  $\log E_t$  and standard deviation (whose units are decades). Note that  $E_t \neq E_k$ , although they turn out to be similar. We show how the numerical results compare to a log-normal distribution in Figure 14. The correspondence is not exact, and the log-normal fit overestimates the high-energy neutrinos while underestimating the low-energy ones. However, it is evidently a decent approximation. The log-normal fit has  $\chi^2 = 0.53$  and  $E_t = 60$  GeV; the fit has  $\chi^2 = 0.49$  and  $E_t = 113$  GeV.

<sup>2</sup> A small number of  $\nu_e$  and  $\nu_\mu$  (as well as  $\nu_\tau$ ) experience repeated neutral-current scatterings without any charged-current scatterings. We neglect this neutral-current-scattered component here, although it is taken into account by our code.

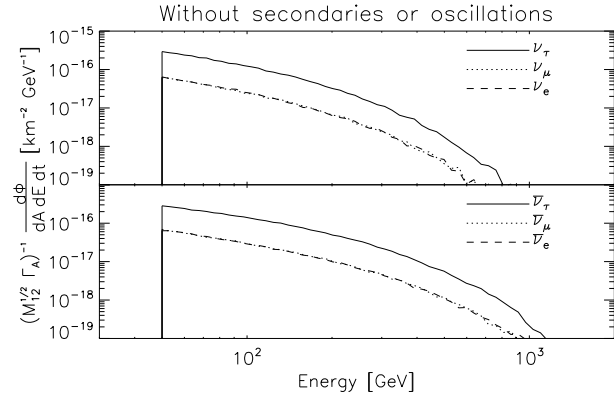


FIG. 13: The simpzilla neutrino fluxes at the Earth, neglecting both neutrino oscillations and secondary neutrinos from decays.

In Figure 15, we plot these analytical approximations. The  $\nu_e$  and  $\nu_\mu$  fluxes are in qualitative agreement with the numerical results. The  $\nu_\tau$  fluxes are somewhat lower at low energies and higher at high energies than are the numerical results, again due to the log-normal underestimating the first while overestimating the second. We note that Eq. (6.5) differs from Eq. (4.6) of [16], leading to a much smaller difference between the  $\nu_\tau$  and  $\nu_e$  event rates; this is due to our correctly taking the  $1=E$  term in the Jacobian factor in the log-normal distribution into account.

The oscillations clearly have a substantial effect on the flux. The  $\nu_\tau$  are depleted, whereas the  $\nu_\mu$  and  $\nu_e$  are enhanced. In a real-world detector, this is advantageous, because it is generally easiest to observe muons from charged-current interactions. The detectability of the simpzilla neutrino flux is therefore improved by oscillations.

In Figure 19, we show the excludable region of simpzilla parameter space; that is, the range of  $m_X$  and  $\chi$  which would be ruled out by the failure to observe a high-energy neutrino signal coming from the direction of the Sun. Even better, of course, would be the observation of such a signal, although further analysis would be necessary to rule out other possible sources such as thermal winds.

## VII. CONCLUSIONS

We have shown that the annihilations of simpzillas in the Sun should produce a conspicuous high-energy neutrino signal in a  $1 \text{ km}^3$  ice detector for a fairly large range of simpzilla mass and interaction cross section. Much of this range of parameter space has not yet been ruled out by current observations.

Our flux calculation takes all important physical effects into account, including neutrino oscillations, which

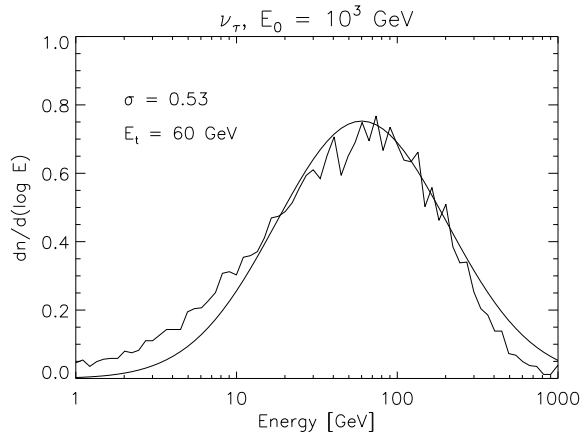


FIG. 14: Distribution of emergent energies for a monoenergetic beam with initial energy  $E_0 = 10^3$  GeV. We have calculated the emergent distribution for other choices of  $E_0$  too, and found it to be generally independent of  $E_0$ . We plot as a distribution in  $\log E$  rather than  $E$ , and neglect oscillations. The distribution corresponds approximately (although obviously not exactly) to the log-normal distribution with the parameters shown.

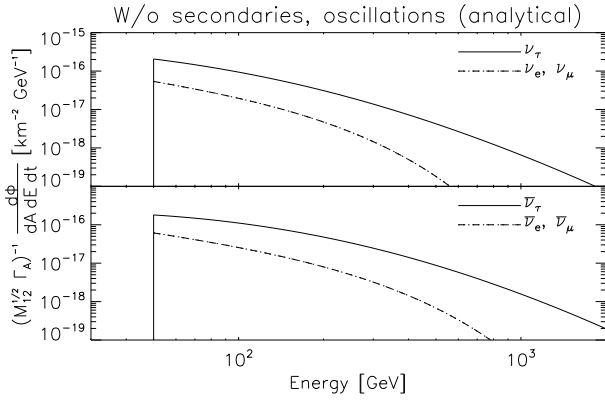


FIG. 15: Analytical approximation for the emergent sim-pzilla neutrino fluxes, neglecting secondaries and oscillations. We assume the  $\nu_e$  and  $\bar{\nu}_e$  fluxes to consist entirely of the remaining unscattered neutrinos, and the  $\nu_\mu$  flux to be the sum of an unscattered component and a scattered component obeying a log-normal distribution. We make similar assumptions about the antineutrinos. The parameters used are given in the text.

approximately equalize the fluxes of the different flavors. In calculating the event rates, we have made some simplifying assumptions about the detector, and a more realistic calculation (say, for IceCube) would take the actual detector response characteristics into account. However, we would not expect this to alter our general conclusion that the sim-pzilla neutrino signal would be observable in such a detector.

The next generation of neutrino detectors should be

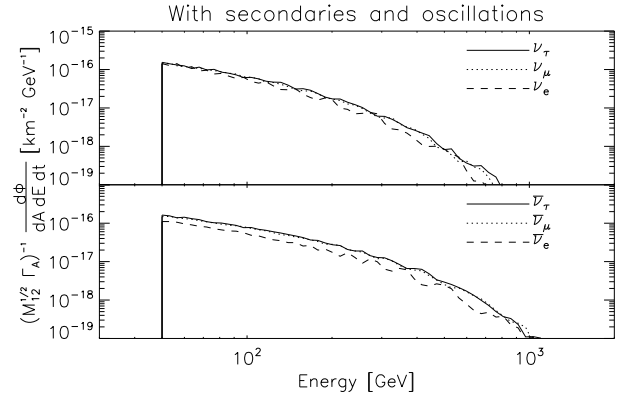


FIG. 16: The sim-pzilla neutrino fluxes at the Earth calculated with our Monte Carlo, taking both oscillations and secondaries into account.

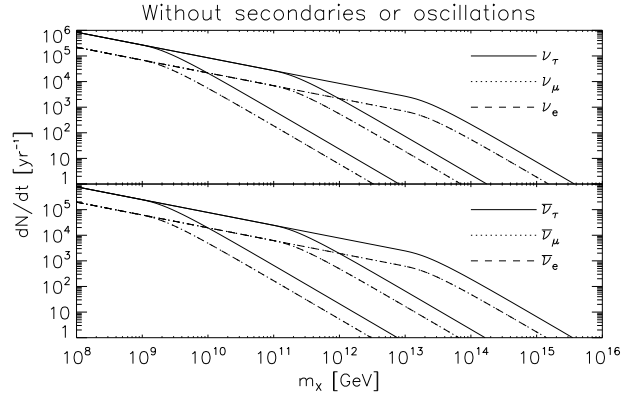


FIG. 17: The sim-pzilla neutrino event rates in a  $1 \text{ km}^3$  idealized detector, neglecting secondaries and oscillations. The rate is plotted as a function of the sim-pzilla mass  $m_x$ . We show three different values for  $\sigma$ , the sim-pzilla interaction cross section: from left to right, these are  $\sigma = 10^{-26} \text{ cm}^2$ ,  $10^{-24} \text{ cm}^2$ , and  $10^{-22} \text{ cm}^2$ . The background from atmospheric neutrinos ( $\nu_e$  and  $\bar{\nu}_e$ ) is approximately  $2 \text{ yr}^{-1}$ . An upper limit from Baksan is about  $10^{-4} \text{ yr}^{-1}$ .

able to either rule out a large range of sim-pzilla parameter space, or provide observational evidence for them.

#### ACKNOWLEDGMENTS

I thank E.W. Kolb for his guidance and support. I also thank J.F. Beacom for assisting me in a large number of ways, and pointing out the phenomenon of neutrino interaction-oscillation decoupling in radius. I thank A.B. Balantekin, A. de Gouvêa, D.E. Groom, D.M. Müller, T.O. Höhne, D. Rainwater, J. Truran, M. Turner, and T. Witten for useful discussions.

I was supported by DOE grant No. 5-90098 while

working on this project.

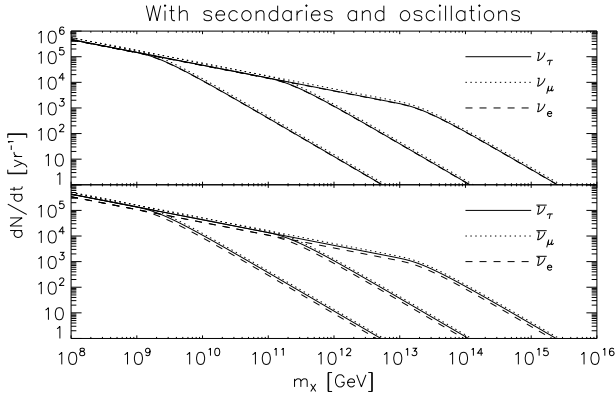


FIG. 18: The simpzilla neutrino event rates, taking both secondaries and oscillations into account. The same choices for are plotted as in Figure 17.

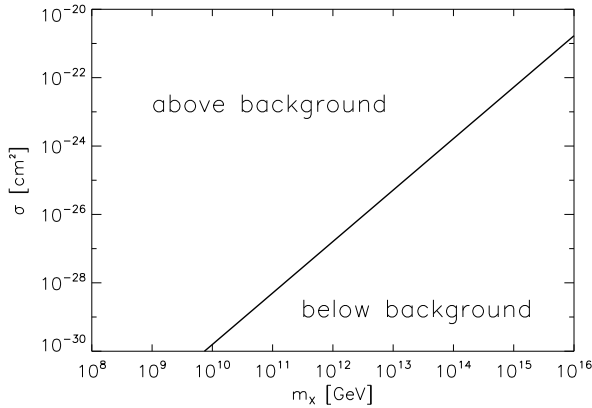


FIG. 19: The regions of simpzilla parameter space which produce neutrino fluxes (in each flavor) that are above and below the background event rate of  $2 \text{ yr}^{-1}$ . If no high-energy neutrino signal is observed from the Sun, it would definitively exclude the range of simpzilla mass and cross section to the left of the line. The plot was generated using the event rates which include both secondaries and oscillations.

---

[1] M. S. Turner, arXiv:astro-ph/0106035.  
 [2] J. Edsjo and P. Gondolo, Phys. Rev. D 56, 1879 (1997) [arXiv:hep-ph/9704361].  
 [3] K. G. Riess and M. Kamionkowski, Phys. Rev. Lett. 64, 615 (1990).  
 [4] W. H. Press and D. N. Spergel, Astrophys. J. 296, 679 (1985).  
 [5] A. Gould, Astrophys. J. 321, 571 (1987).  
 [6] S. Ritz and D. Seckel, Nucl. Phys. B 304, 877 (1988).  
 [7] D. J. Chung, E. W. Kolb and A. Riotto, Phys. Rev. D 59, 023501 (1999) [arXiv:hep-ph/9802238].  
 [8] D. J. Chung, E. W. Kolb and A. Riotto, Phys. Rev. Lett. 81, 4048 (1998) [arXiv:hep-ph/9805473].  
 [9] D. J. Chung, E. W. Kolb and A. Riotto, Phys. Rev. D 60, 063504 (1999) [arXiv:hep-ph/9809453].  
 [10] E. W. Kolb, D. J. Chung and A. Riotto, arXiv:hep-ph/9810361.  
 [11] V. Kuzmin and I. Tkachev, Phys. Rev. D 59, 123006 (1999) [arXiv:hep-ph/9809547].  
 [12] D. J. Chung, arXiv:hep-ph/9809489.  
 [13] D. J. Chung, P. Crotty, E. W. Kolb and A. Riotto, Phys. Rev. D 64, 043503 (2001) [arXiv:hep-ph/0104100].  
 [14] A. Gould, B. T. Durrance, R. W. Romani and S. Nussinov, Phys. Lett. B 238, 337 (1990).  
 [15] E. Nardi and E. Roulet, Phys. Lett. B 245, 105 (1990).  
 [16] I. F. Albuquerque, L. Hu and E. W. Kolb, Phys. Rev. D 64, 083504 (2001) [arXiv:hep-ph/0009017].  
 [17] C. T. Hill, Nucl. Phys. B 224, 469 (1983).

[18] J. Ahrens et al., *IceCube Preliminary Design Document* (IceCube Collaboration, 2001).

[19] R. Gandhi, C. Quigg, M. H. Reno and I. Sarcevic, *Astropart. Phys.* 5, 81 (1996) [[arXiv:hep-ph/9512364](#)].

[20] R. Gandhi, C. Quigg, M. H. Reno and I. Sarcevic, *Phys. Rev. D* 58, 093009 (1998) [[arXiv:hep-ph/9807264](#)].

[21] J. N. Bahcall, *Neutrino Astrophysics* (Cambridge University Press, Cambridge, U.K., 1989).

[22] J. Pumplin, D. R. Stump, J. Huston, H. L. Lai, P. Nadecky and W. K. Tung, [arXiv:hep-ph/0201195](#).

[23] E. A. Paschos and J. Y. Yu, *Phys. Rev. D* 65, 033002 (2002) [[arXiv:hep-ph/0107261](#)].

[24] M. Kowalski, *Phys. Lett. B* 511, 119 (2001) [[arXiv:hep-ph/0009183](#)].

[25] F. Halzen and D. Saltzberg, *Phys. Rev. Lett.* 81, 4305 (1998) [[arXiv:hep-ph/9804354](#)].

[26] S. I. Dutta, M. H. Reno and I. Sarcevic, *Phys. Rev. D* 62, 123001 (2000) [[arXiv:hep-ph/0005310](#)].

[27] F. Becattini and S. Bottai, *Astropart. Phys.* 15, 323 (2001) [[arXiv:astro-ph/0003179](#)].

[28] J. F. Beacom, P. Crotty and E. W. Kolb, [arXiv:astro-ph/0111482](#).

[29] S. I. Dutta, M. H. Reno, I. Sarcevic and D. Seckel, *Phys. Rev. D* 63, 094020 (2001) [[arXiv:hep-ph/0012350](#)].

[30] D. E. Groom et al. [Particle Data Group Collaboration], *Eur. Phys. J. C* 15, 1 (2000).

[31] D. E. Groom, N. V. Mokhov and S. I. Striganov, *Atom. Data Nucl. Data Tabl.* 78, 183 (2001).

[32] P. Renton, *Electroweak Interactions* (Cambridge University Press, Cambridge, U.K., 1990).

[33] Y. Fukuda et al. [Super-Kamiokande Collaboration], *Phys. Rev. Lett.* 81, 1562 (1998) [[arXiv:hep-ex/9807003](#)].

[34] S. Fukuda et al. [Super-Kamiokande Collaboration], *Phys. Rev. Lett.* 85, 3999 (2000) [[arXiv:hep-ex/0009001](#)].

[35] A. de Gouvea, *Phys. Rev. D* 63, 093003 (2001) [[arXiv:hep-ph/0006157](#)].

[36] J. R. Klein [SNO Collaboration], [arXiv:hep-ex/0111040](#).

[37] Q. R. Ahmad et al. [SNO Collaboration], [arXiv:nucl-ex/0204008](#).

[38] Q. R. Ahmad et al. [SNO Collaboration], [arXiv:nucl-ex/0204009](#).

[39] P. I. Krastev and A. Y. Smirnov, *Phys. Rev. D* 65, 073022 (2002) [[arXiv:hep-ph/0108177](#)].

[40] T. Ohlsson and H. Snellman, *J. Math. Phys.* 41, 2768 (2000) [Erratum *ibid.* 42, 2345 (2000)] [[arXiv:hep-ph/9910546](#)].

[41] T. Ohlsson and H. Snellman, *Eur. Phys. J. C* 20, 507 (2001) [[arXiv:hep-ph/0103252](#)].

[42] I. F. Albuquerque, J. Lamoureux and G. F. Smoot, [arXiv:hep-ph/0109177](#).

[43] M. M. Boliev, E. V. Bugaev, A. V. Butkevich, A. E. Chudakov, S. P. Mikhnevich, O. V. Suvorova and V. N. Zakidyshev, *Nucl. Phys. Proc. Suppl.* 48, 83 (1996).

[44] R. W.ischnewski et al., *Nucl. Phys. Proc. Suppl.* 75A, 412 (1999).

[45] I. F. Albuquerque, J. Lamoureux and G. F. Smoot, [arXiv:hep-ph/0204301](#).